



Deposited via The University of Sheffield.

White Rose Research Online URL for this paper:

<https://eprints.whiterose.ac.uk/id/eprint/118036/>

Version: Accepted Version

---

**Article:**

Li, J., Wasley, T., Ta, D. et al. (2018) Micro electronic systems via multifunctional additive manufacturing. *Rapid Prototyping Journal*, 24 (4). ISSN: 1355-2546

<https://doi.org/10.1108/RPJ-02-2017-0033>

---

**Reuse**

This article is distributed under the terms of the Creative Commons Attribution-NonCommercial (CC BY-NC) licence. This licence allows you to remix, tweak, and build upon this work non-commercially, and any new works must also acknowledge the authors and be non-commercial. You don't have to license any derivative works on the same terms. More information and the full terms of the licence here:

<https://creativecommons.org/licenses/>

**Takedown**

If you consider content in White Rose Research Online to be in breach of UK law, please notify us by emailing [eprints@whiterose.ac.uk](mailto:eprints@whiterose.ac.uk) including the URL of the record and the reason for the withdrawal request.



**Micro Electronic Systems via Multifunctional Additive Manufacturing**

Journal:	<i>Rapid Prototyping Journal</i>
Manuscript ID	RPJ-02-2017-0033.R1
Manuscript Type:	Original Article
Keywords:	Additive Manufacturing, DLP Stereolithography, Material Dispensing, Multilayer Embedded Electronics, Flip Chip Packaging, Process Integration

SCHOLARONE™  
Manuscripts

# Micro Electronic Systems via Multifunctional Additive Manufacturing

## Abstract

**Purpose** – This paper aims to demonstrate the innovative functionality of additive manufacturing technology provided by combining multiple processes for the fabrication of packaged electronics.

**Design/Methodology/Approach** – This research is focused on the improvement in resolution of conductor deposition methods through experimentation with build parameters. Material dispensing with two different low temperature curing isotropic conductive adhesive materials were characterised for their application in printing each of three different conductor designs, traces, z-axis connections and fine pitch flip chip interconnects. Once optimised, demonstrator size can be minimised within the limitations of the chosen processes and materials.

**Findings** – The proposed method of printing z-axis through layer connections was successful with pillars 2mm in height and 550 $\mu$ m in width produced. Dispensing characterisation also resulted in tracks 134 $\mu$ m in width and 38 $\mu$ m in height allowing surface mount assembly of 0603 components and thin-shrink small outline packaged integrated circuits. Small 149 $\mu$ m flip chip interconnects deposited at a 457 $\mu$ m pitch have also been used for packaging silicon bare die.

**Originality/Value** – This paper presents an improved multifunctional additive manufacturing method to produce fully packaged multilayer electronic systems. It discusses the development of new 3D printed, through layer z-axis connections and the use of a single electrically conductive adhesive material to produce all conductors. This facilitates the surface mount assembly of components directly onto these conductors before Stereolithography is used to fully package multiple layers of circuitry in a photopolymer.

**Keywords** Additive Manufacturing, Process Integration, DLP Stereolithography, Material Dispensing, Multilayer Embedded Electronics, Flip Chip Packaging

**Paper Type** Research Paper

## Introduction

Electronics manufacturing techniques require a wide range of materials including conductors and dielectrics to generate complex circuitry. These processes are characteristically wasteful and their template driven nature requires volume production to achieve economic viability. This results in long pre-production timescales and a lack of customisation and versatility.

1  
2  
3 Additive Manufacturing (AM) technologies, commonly termed 3D printing, have been introduced as  
4 an innovative alternative to a variety of traditional manufacturing technologies (Sharma 2014)(Anon  
5 2012). They provide benefits such as waste reduction, increased geometric freedom and digitally  
6 driven fabrication directly from a CAD model, making templates and moulds obsolete. Until recently,  
7 AM research and development has been focused on individual processes and materials, therefore  
8 adopting their inherent limitations. To encourage 3D printing technology to reach its full potential,  
9 multiple processes area being combined to create functional products from numerous materials.  
10 Favourable characteristics of AM techniques can be combined with a range of material possibilities  
11 to provide increased functionality in an array of applications (Lipson & Kurman 2013) such as  
12 microfluidics, embedded sensor systems and electronic packaging.  
13  
14  
15  
16  
17  
18

19  
20 A variety of AM processes have been hybridised to challenge traditional electronics manufacturing  
21 technologies including combinations of both ultrasonic consolidation (A. J. Lopes et al. 2006) and  
22 stereolithography (Lopes et al. 2012) with direct writing.  
23  
24

25  
26 A concept was introduced for the encapsulation of a printed circuit board (PCB) within a package  
27 fabricated using stereolithography (Niese et al. 2014). Off-axis vias were added to the package to  
28 route power to the PCB, and were to be created using the Additive 3D Molded Interconnect Device  
29 (ADDMID) process. Laser processing of the doped photopolymer resin allows ablated structures to  
30 be metallised through the exposure of coated aluminium particles.  
31  
32  
33

34  
35 The fabrication of electronics using a hybrid stereolithography and direct writing approach was first  
36 proven by The University of Texas at El Paso, who first demonstrated the compatibility between  
37 conductive materials and photopolymer materials (Palmer et al. 2004). Photopolymer substrates  
38 with trenches and off-axis tunnels were fabricated using a top down laser based stereolithography  
39 technique. Through hole components were placed in trenches which were then filled with liquid  
40 photopolymer and cured, leaving a network of channels on the surface to contain the conductive ink  
41 (A. Lopes et al. 2006). Direct write technologies were used to deposit low viscosity conductive inks  
42 into the channels and the ink was also pumped into the tunnels, allowing conductive channels to  
43 cross without intersection. Conductive traces were deposited in channels and components housed in  
44 individual trenches on the substrate surface. The compatibility of this approach with surface mount  
45 technology is limited, resulting in a larger electronic footprint and in addition, the production of  
46 circuitry was restricted to the surface of the part with specific structural features required to control  
47 conductor deposition.  
48  
49  
50  
51  
52  
53  
54  
55  
56  
57  
58  
59  
60

1  
2  
3 Aerosol jetting has been applied to the printing of conductors on 3D printed plastic surfaces. In 2012,  
4 Fused Deposition Modelling and aerosol jetting were interleaved by Optomec and Stratasys to print  
5 functional strain gauges and conductors to generate electric power for the propeller engine of an  
6 unmanned aerial vehicle (Paulsen et al. 2012). Circuitry with a resolution of 10µm was produced  
7 onto three dimensional surfaces however, this process was again limited to post processing of a pre-  
8 fabricated substrate.  
9

10  
11  
12  
13  
14  
15  
16  
17  
18  
19  
20  
21  
22  
23  
24  
25  
26  
27  
28  
29  
30  
31  
32  
33  
34  
35  
36  
37  
38  
39  
40  
41  
42  
43  
44  
45  
46  
47  
48  
49  
50  
51  
52  
53  
54  
55  
56  
57  
58  
59  
60  
Voxel8 released a hybrid system combining both Fused Filament Fabrication (FFF) and dispensing  
within one material extrusion machine in 2016 (Borghino 2015). This allows the simultaneous  
printing of substrates and electronic circuits to produce functional electronic structures. The  
resolution of the FFF process is typically limited to 0.8mm features in the x and y axes due to the  
0.4mm diameter nozzle and suffers from stair stepping issues in the z-axis due to the large layer  
thicknesses. Despite the advantages of the multi-material process the dimensional capabilities of the  
system are limited by the choice of processes.

In this paper a manufacturing process combining direct light projection (DLP) based  
Stereolithography (SL) and direct write (DW) technology is presented, allowing the production of  
fully functional multilayer electronic systems directly from a digital model. This combination of  
manufacturing techniques coupled with mid-process cleaning, electronic surface mount component  
assembly and thermal curing provides the multi-material, multi-process functionality required to  
produce high quality, high density electronics packaged in geometrically complex structures.

## Hybrid Manufacturing Process, Apparatus and Materials

### Manufacturing Process

The manufacturing process chain has been detailed in Figure 1. It begins with substrate fabrication  
via bottom up DLP Stereolithography, creating a base in a layer-by-layer build method. After  
ultrasonic agitation to remove excess liquid photopolymer, isotropic conductive adhesives (ICAs) are  
selectively dispensed onto the clean substrate surface to simultaneously produce conductive tracks,  
surface mounted device (SMD) interconnects and novel z-axis through layer connections in the form  
of freestanding pillar structures. Surface mount component assembly is then conducted onto  
deposited interconnects before exposure to a low temperature in a thermal oven to cure the ICA  
without degrading the substrate material. Finally, the electronics are embedded through a single  
long period of exposure to a projected UV image, resulting in small protrusions of pillar tips through  
the layer as well as providing a flat surface for subsequent electronic dispensing. Stages (b) to (e) in

1  
2  
3 Figure 1 can be repeated multiple times to produce a fully packaged multilayer electronic system  
4 (Figure 1(h)).  
5  
6  
7

8 Figure 1. Overview of the multifunctional additive manufacturing process  
9

### 10 Stereolithography System

11 Digital light projection (DLP) Stereolithography (SL) is an Additive Manufacturing (AM) process that  
12 fabricates three dimensions parts from a liquid photopolymer by selectively curing multiple thin  
13 layers of material one on top of the other (Hull 1986). This method differs from laser based  
14 Stereolithography processes as the photopolymerisation is achieved by exposing a single layer of  
15 photosensitive resin to a projected image for a predetermined period of time. DLP projection can be  
16 orientated downwards or upwards, the latter has been utilized in this integrated process. A  
17 projection system is positioned underneath the vat with a transparent base and antistiction  
18 polydimethyl-siloxane (PDMS) coating, with the projection lens positioned and focused on the centre  
19 of the base. This method builds parts upside down, producing a surface high quality surface finish as  
20 it is polymerised in contact with the PDMS layer (Zhou et al. 2013).  
21

22 A mUve 1.5 DLP system from mUve3D was modified to improve its structural rigidity, allowing the  
23 process to be paused, parts removed and, reinserted in an identical location. A 405nm ultraviolet  
24 projection source, DLP Lightcrafter™ 4500 projection module from Texas Instruments, was added  
25 with a resolution of 109µm over a 140mm x 87mm projection area. The light density of the projector  
26 was measured at 3.16mW/cm<sup>2</sup> at the lens, and an average of 0.98mW/cm<sup>2</sup> at the point of  
27 interaction with the photopolymer using an International Light IL1400A UV light meter. The single-  
28 wavelength ultraviolet light source reduced the stresses on the substrates caused by absorption of a  
29 wide range of wavelengths emitted from a white light source. Manual micrometre height control of  
30 the build platform height was incorporated ensuring that the layer thickness was kept constant and  
31 the home position could be accurately altered. This bespoke DLP Stereolithography apparatus with  
32 bottom up UV projection orientation was used to produce the base photopolymer substrates with a  
33 layer thickness of 100µm. To produce a complex package, geometrically intricate external walls can  
34 be fabricated creating a cavity to contain the layer of deposited circuitry. Once the SLA build stage  
35 has finished, the part can be subjected to ultrasonic agitation in a solvent, removing all excess  
36 uncured photopolymer before being dried by a clean compressed air source.  
37  
38  
39  
40  
41  
42  
43  
44  
45  
46  
47  
48  
49  
50  
51  
52  
53

### 54 Liquid Photopolymer Materials

55 Liquid photopolymers are all sensitive to light however, different photoinitiators can change the  
56 wavelength of light to which the material is sensitive. To initiate polymerisation the energy of light  
57  
58  
59  
60

1  
2  
3 exposure must breach the activation energy of the initiator (Andrzejewska 2001)(Gruber 1992).  
4 Traditional, commercial laser based SL systems contain high power 365nm lasers and therefore,  
5 commercial resins are designed to polymerise when exposed to this wavelength and intensity of  
6 light. The integration of a 365nm light source into a DLP projector resulted in too low an intensity. A  
7 405nm light source in the form of a Texas Instruments DLP Lightcrafter™ 4500 Evaluation Module  
8 was used. MakerJuice SF resin from MakerJuice Labs was selected for its low stress behaviour under  
9 UV light and heat exposure, its visible clarity and high resolution capability.  
10

### 11 Dispensing System

12 Dispensing is one of a variety of direct writing methods by which conductors can be deposited onto a  
13 photopolymer surface. A Musashi Shotmaster500 dispensing system capable of high resolution  
14 automated movement was used to deposit silver filled conductive materials. The pneumatic  
15 pressure produced by the Musashi SuperΣCMII digital control dispenser makes it compatible with  
16 high viscosity materials, therefore facilitating the printing of high load silver filled materials to  
17 produce conductors. In addition, the process is fully digitally driven with dedicated MuCAD software  
18 enabling the design and control of dispensing patterns, machine movement and printing parameters.  
19 This system is capable of printing at speeds between 0.1mm/s and 300mm/s and pressures between  
20 30kPa and 500kPa which, when combined with regulation of nozzle size, print gap and material  
21 characteristics, make this process highly controllable. Traditionally z-axis connections in electronics  
22 manufacturing are produced by a combination of subtractive and additive methods. Through the use  
23 of AM a hole can be fabricated layer by layer without subtractive machining methods however; the  
24 method of encapsulation introduced in this paper prevents the creation of a deep, high resolution  
25 via holes. A novel method of connecting multiple layers of circuitry was therefore developed  
26 resulting in three dimensional, freestanding pillars that could be embedded, leaving a 50µm peak  
27 exposed to contact subsequent layers of circuitry. These z-axis through-layer connections were  
28 deposited simultaneously with conductive tracks and SMD interconnects in one automated process.  
29  
30  
31  
32  
33  
34  
35  
36  
37  
38  
39  
40  
41  
42  
43  
44

### 45 Conductive Materials

46 Epotek® E4110-PFC and EJ2189 silver filled ICAs with maximum particle sizes of  $\leq 20\mu\text{m}$  and  $\leq 45\mu\text{m}$   
47 were selected for experimentation for three reasons. Firstly, they cure at low temperature, below  
48 the glass transition temperature of the photopolymer substrates, secondly, they have a high  
49 viscosity, ensuring the deposition can be controlled and structures will maintain their desired shape  
50 and finally, can be used to produce all conductors simultaneously in these embedded structures.  
51 These material properties are listed in Table 1. Both candidate epoxies can be thermally cured at  
52 temperatures ranging from room temperature (23°C) to 150°C, however, the liquid photopolymer  
53 limited this curing temperature to a maximum of 100°C before the substrate degraded. However,  
54  
55  
56  
57  
58  
59  
60

1  
2  
3 due to the lower glass transfer temperature  $T_g$  of cured SL resin (MakerJuice SF) the curing  
4 temperature of both conductive epoxies was limited to 100 °C. Any higher curing temperature  
5 resulted in the SL substrate degrades that caused cracking and partial delamination of the very top  
6 surface.  
7  
8  
9

10  
11 Table 1. Important properties of chosen conductive materials according to Epotek specifications  
12

### 13 14 15 Electronic Packaging

16 The use of isotropic conductive adhesive materials to fabricate conductors makes this dispensing  
17 process and materials compatible with surface mount assembly (SMA). SMA is the most commonly  
18 used packaging method for mounting components directly onto printed circuit boards due to its high  
19 density capability, high throughput and low cost. Components can be placed directly onto dispensed  
20 ICA interconnects. The final stage in the deposition of electronics is low temperature thermal curing.  
21 A regime of 80°C for 3 hours was used to prevent degradation of the substrate, resulting in an  
22 approximate volume resistivity of  $7 \times 10^{-4} \Omega \text{cm}$  in both materials. According to Table 1, when both  
23 conductive epoxies are fully cured, their resistivity should be less than 5 m $\Omega$  cm. The experimental  
24 samples measured resistivity was in this expected range.  
25  
26  
27  
28  
29  
30

31 The SL apparatus is used to package each circuit layer individually. With or without a cavity,  
32 embedding of electronics is conducted by re-inserting the build platform with attached specimen  
33 into the material vat, pressing the top 100 $\mu\text{m}$  of the pillars into the non-stick PDMS layer and flood  
34 exposing the thick layer of photopolymer. To prevent the formation of bubbles in the cavity, it is  
35 filled facing upwards, the air is left to settle out and the wetted part is then inserted into the SL  
36 apparatus. This process can then be repeated creating multiple embedded layers in a geometrically  
37 complex package. The thickness of these layers is determined by the height of the tallest  
38 components and therefore layers 2mm and 1.2mm in thickness were proposed for 1206 and 0603  
39 (imperial code) surface mount devices.  
40  
41  
42  
43  
44  
45

46 Packaging can also be conducted on a chip scale. Figure 2 shows the difference between the  
47 traditional and AM methods of flip chip packaging daisy chain patterned bare die, the example used  
48 in this feasibility test. Flip chip packaging allows bare microchips to be attached face down onto a  
49 substrate with a smaller pitch between the array of bond pads facilitating a higher input/output  
50 density. This technique is an evolution of SMA and reduces substrate weight in addition to making  
51 the device thinner. Conventional copper tracks and solder bumps can be replaced with ICA filled  
52 channels in the substrate and printed interconnects. In addition the photopolymer is used to fully  
53 encapsulate the chip acting as both the insulating underfill and package.  
54  
55  
56  
57  
58  
59  
60

Figure 2. Comparison of flip chip packaging via a) conventional methods and b) multifunctional additive manufacturing

Photopolymers substrates were fabricated with surface trenches before being cleaned and filled with isotropic conductive adhesive. Once cured, the surface was planarised using a polishing process before fine pitch interconnects were deposited onto each end of the sub-surface trenches. Alignment of the interconnects with metallised tracks and pads on the underside of the chip can was conducted using a Leica Wild M3Z optical beam splitting microscope with manual micrometre alignment before a rotating placement arm was used to place the chip in position.

### Development and Experimental Miniaturisation of Conductors

To facilitate the shrinking of the footprint of electronic systems produced using AM methods, the density of printed conductors required increasing. Systematic experimentation of different dispensing parameters was conducted to determine the combination required to produce the smallest uniform traces and z-axis connecting pillars. The miniaturisation of these systems was also reliant on the compatibility of this dispensing process with smaller surface mount components and integrated circuits, requiring the pitch of dispensed features to be reduced.

The selected ICA materials were the limiting factor in this investigation, with their maximum particle sizes limiting the inner diameter (ID) of the nozzles through which they could be deposited. There is a rule of thumb from ICA suppliers that the nozzle diameter should be 5 times larger than the maximum particle size to avoid any clogging. For Epotek® E4110-PFC, the maximum particle size was 20µm (Table 1), and thus the nozzle ID was limited to 100µm. 200µm and 250µm ID nozzle were also utilised in this work for comparison.

#### Conductive Tracks

Three printing parameters were identified as having the greatest influence on the track profile, specifically the width as it is the most influential parameter for the reduction of the dispensing pitch and therefore miniaturisation. An array of tracks was produced using two epoxies and a combination of three experimental variables, nozzle inner diameter, printing pressure and print speed. A range of suitable printing pressures for material A (100kPa to 450kPa) and material B (30kPa to 180kPa) and, print speeds (1mm/s to 7mm/s) were determined during a preliminary investigation. Values outside these ranges resulted in poor track quality, lack of wetting to the substrate or an excessive volume of deposited material. An Alicona InfiniteFocus® G4f non-contact variation focus microscopy system with a x10 object lens was used to scan the profile and extract trace height, width and cross sectional area.

1  
2  
3 Track widths resulting from deposition in material A were analysed and are presented in Figure 3(a).  
4 In addition, Figure 3(b)-(d) presents a matrix of track profiles showing the effect of print parameters  
5 on their appearance. Smaller track widths and heights were achieved by reducing nozzle ID,  
6 decreasing print pressure and increasing print speed however, to print material A through the  
7 narrowest 100 $\mu\text{m}$  nozzle, a minimum print pressure of 250kPa was required. The narrowest uniform  
8 trace was produced using a nozzle ID of 100 $\mu\text{m}$ , printing pressure of 300kPa and speed of 7mm/s  
9 and, measured 170 $\mu\text{m}$  in width and 43 $\mu\text{m}$  in height. By comparison, the 200 $\mu\text{m}$  and 250 $\mu\text{m}$  IDs  
10 resulted in minimum trace widths of 304 $\mu\text{m}$  and 352 $\mu\text{m}$ .  
11  
12  
13  
14  
15  
16  
17  
18  
19

Figure 3. Effect of printing parameters on track width and appearance of material A

20  
21 Material B exhibited the same behaviour however, due to its lower viscosity, printing pressures  
22 ranged between 30kPa and 90kPa and, trace width increased at a greater rate with pressure as  
23 shown in Figure 4(a).  
24  
25

26 A comparison of Figure 4(b)-(d) with the material A track matrix shows that trace profiles produced  
27 in material A are smoother than material B. This has been attributed to its higher viscosity resulting  
28 in less solvent evaporation during thermal curing and its smaller particle size. Tracks of the same  
29 height printed in both ICAs demonstrated that material A produced samples up to 20% narrower  
30 than material B due its higher viscosity however, a larger pressure was required that may result in  
31 larger volumes of material deposited. Material B was able to produce the smallest track profile with  
32 a width of 134 $\mu\text{m}$  and height of 38 $\mu\text{m}$ , realised through a 100 $\mu\text{m}$  nozzle orifice using a pressure of  
33 140kPa and speed of 7mm/s. The lower viscosity material separates more easily from the nozzle  
34 orifice and in combination with a lower printing pressure, allowed smaller volumes of ICA to be  
35 deposited.  
36  
37  
38  
39  
40  
41  
42  
43  
44

Figure 4. Effect of printing parameters on track width and appearance of material B

#### 45 46 47 Z-axis through Layer Conductors

48 Minimising the footprint of the z-axis interconnects is contingent on a compromise between the  
49 base diameter and the stability of the structure. With increasing base diameter, the achievable  
50 height of the pillar increases. Preliminary testing was conducted to design the tool path and  
51 dimensions of the pillars and, identifies the limits of print speed and pressure. Individual design files  
52 with dimensions proportional to each nozzle ID, shown in Figure 5, were produced to allow the  
53 aspect ratios of printed structures to be compared to one another.  
54  
55  
56  
57  
58  
59  
60

Figure 5. Freestanding pillar designs for each nozzle ID

The freestanding nature of these z-axis interconnecting pillars required a high aspect ratio to be achieved. A comparison of the height, diameter and aspect ratio of pillars produced using the two candidate ICAs is presented in Figure 6. Structures printed through 250 $\mu$ m and 200 $\mu$ m nozzle IDs resulted in material A pillars on average 32% (~2mm) and 15% (~1.7mm) higher than material B. Pillar diameters are similar at lower pressures however, these diameters increase more rapidly with pressure in material B, peaking with a difference in diameter of 28% with the 250 $\mu$ m nozzle and 13% with the 200 $\mu$ m nozzle which, when combined with the pillar heights, create higher aspect ratios in material A structures.

Figure 6. Diameters, height and aspect ratios of pillars produced in materials A and B using 250 $\mu$ m and 200 $\mu$ m nozzle IDs

Following this preliminary investigation material B was discounted for use in pillar dispensing due to its slumping behaviour which is exaggerated by higher volume deposition and the weight of sequentially stacked layers. Experimentation with material A was undertaken to identify the relationship between nozzle size, dispensing speed and dispensing pressure on the height and diameter of pillars measured using an Alicona InfiniteFocus® G4f non-contact variation focus microscopy system. With an experimental mandate to minimise the diameter of the pillars and ensure enough height to connect circuit layers a maximum acceptable value of base diameter was set at 1mm. Figure 7(a) and (b) shows the effect of changing nozzle ID, print speed and printing pressure on the diameter and height of printed pillars. The visual effect of decreasing pressure, nozzle ID and print speed on pillar appearance are also shown in Figure 7(c)-(e). Diameter increases quickly with pressure however, as the height is largely determined by the design height, it only increases by small increments due to the higher volume of deposited material. In addition, increasing speed reduced both the track width and the height. Finally, larger nozzles also resulted in higher volume deposition and therefore wider and taller conductors.

Figure 7. Graphic representation of effect of changing printing parameters on a) diameter and b) height of profiles produced with decreasing c) pressures, d) nozzle sizes and e) print speeds

The highest aspect ratio achieved during this investigation was 2.26 at a height of ~1.5mm and diameter of ~0.67mm using a 200 $\mu$ m nozzle ID at a pressure of 80kPa and print speed of 7mm/s. The 100 $\mu$ m nozzle produced the smallest pillar base diameter of ~0.5mm however with a height of

1  
2  
3 ~0.7mm the aspect ratio is limited to 1.4. This characteristic would therefore prevent this structure  
4 from forming a connection through the 1.2mm thick embedding layers proposed for packaging of  
5 0603 surface mount devices without additional layers added to the design.  
6  
7

8  
9 Additional iterative experimental changes to the height of the pillar design were made to create the  
10 tallest structure possible with a maximum diameter of approximately 1mm. Using the more viscous  
11 material A and a 250 $\mu$ m nozzle ID, printing pressure of 90kPa and print speed of 4mm/s, a height of  
12 3.8mm and width of 0.9mm was achieved over 16 printed layers. A maximum of 18 layers could be  
13 printed through a 200 $\mu$ m nozzle and 24 were achieved through a 100 $\mu$ m nozzle. Figure 8  
14 summarises these results and shows a comparison with material B.  
15  
16  
17  
18  
19

20  
21 Figure 8. Comparison of largest achievable pillar structures using a combination of two materials and three nozzle sizes  
22  
23

24  
25 Material A and a 100 $\mu$ m nozzle ID produced the narrowest pillar diameter whilst measuring over  
26 2mm in height. Although its measured aspect ratio, 3.67, is smaller than its 250 $\mu$ m nozzle equivalent,  
27 3.81, packages were designed with a maximum 2mm layer thickness therefore making the 100 $\mu$ m  
28 nozzle most suitable as it produced the narrowest pillar diameter while meeting the height  
29 requirement.  
30  
31  
32

### 33 *Interconnect Dispensing for Flip Chip Packaging*

34  
35 The miniaturisation of electronic packaging is contingent on the integration of smaller packaging  
36 technology with this multifunctional additive manufacturing process, facilitating the demonstration of  
37 chip scale packaging. This required the deposition of interconnecting conductive bumps onto  
38 photopolymer substrates at a narrow pitch. Interconnect features were achieved by locating the  
39 nozzle at a designed location, with a given print gap and pressure and, dispensing was actuated for a  
40 pre-determined period of time. The resulting bumps were then scanned using the Alicona  
41 microscope to analyse the topography. Preliminary experimentation provided a range of pressures,  
42 print gaps and actuation times for both materials through a 200 $\mu$ m nozzle. The achievable feature  
43 sizes of the two epoxies were compared at a 0.3 second actuation time and 100 $\mu$ m print gap to  
44 determine their suitability for this process. Figure 9(a) shows that feature diameters 100 $\mu$ m  
45 narrower have been achieved using material B, a result of the lower viscosity and therefore lower  
46 pressure required to print these features. Pressure values below the minimum shown are either a  
47 restriction of the dispensing system or result in no material flow. Material A displays greater error  
48 and printing inconsistency, demonstrating sub-optimal results for use in chip scale packaging.  
49  
50  
51  
52  
53  
54  
55  
56  
57  
58  
59  
60

1  
2  
3 Material A also produces higher, sharper peaks shown in Figure 9(b), resulting in a greater chip  
4 standoff distance and a higher volume of dispensed material, therefore making material B more  
5 suitable.  
6  
7

8  
9  
10 Figure 9. Comparison of interconnects printed in materials A and B  
11

12  
13 Figure 10 shows the systematic investigation of material B over a range of pressure actuation times  
14 to determine the optimum parameters for the production of the smallest possible consistently  
15 deposited feature. The smallest diameter produced through the 200 $\mu\text{m}$  nozzle was 259 $\mu\text{m}$  while this  
16 dimension was reduced to 149 $\mu\text{m}$  through a 100 $\mu\text{m}$  nozzle. The smallest ICA bumps were produced  
17 at a print gap of 60 $\mu\text{m}$  with values both above and below resulting in insufficient adhesion to the  
18 substrate and increased spreading of the epoxy respectively.  
19  
20  
21  
22

23  
24  
25  
26 Figure 10. Relationship between printing pressure, actuation time and bump diameter at a 60 $\mu\text{m}$  print gap with a 100 $\mu\text{m}$  nozzle in  
27 material B  
28

29  
30 Interconnects with a diameter of 150 $\mu\text{m}$  showed high repeatability, proving that the production of  
31 fine pitch interconnects is possible using additive manufacturing technology and therefore  
32 facilitating the combination of this deposition technique with substrate manufacturing methods.  
33  
34

### 35 36 **Demonstrators**

#### 37 *Multilayer 555 Timer*

38  
39 A flashing 555 timer circuit was chosen to demonstrate the capability of this multi-process  
40 manufacturing technique for embedded electronics. The three layer design was incorporated into a  
41 pyramid to exhibit the potential of this technique to develop packages with higher geometric  
42 complexity. Figure 11 presents the iterative miniaturisation of this three layer demonstrator as a  
43 result of the dispensing process characterisation and reduction in SMD and IC dimensions. The two  
44 examples show a reducing substrate base width from 30mm x 30mm to 15mm x 15mm made  
45 possible by decreasing the footprint of the electronics from 12mm x 12mm to 8mm x 8mm.  
46  
47  
48  
49  
50  
51  
52  
53

54 Figure 11. Comparison of demonstrator size reduction across three iterations  
55  
56  
57  
58  
59  
60

1  
2  
3 Figure 11(a) and (b) demonstrate the 50% reduction in size of surface mount devices (from 1206  
4 package to 0603 package) and packaging of a 4.4mm x 3mm x 1.2mm thin-shrink small outline  
5 package (TSSOP) with a pitch of 650 $\mu$ m between pins, condensed from a 4.9mm x 3.9mm x 1.75mm  
6 mini small outline package (MSOP) with a pitch of 1.27mm between pins. This facilitated the  
7 reduction in embedding layer thickness from 2mm to 1.2mm. The dispensing parameters also  
8 changed resulting in the use of a 100 $\mu$ m nozzle to produce circuitry on the smaller substrate while a  
9 250 $\mu$ m nozzle had previously been used to produce the larger iteration.  
10  
11  
12  
13

#### 14 *Flip Chip Packaging*

15  
16 A 6.3mm x 6.3mm daisy chain bare die with pre-bumped metallised pads was packaged using  
17 multifunctional additive manufacturing techniques. Ideally these pads would not have solder on them  
18 as it increases the standoff height and contact resistance however, a polishing process was used to  
19 remove the majority of the solder to more accurately simulate the packaging of a bump-free chip.  
20 The pads are 195 $\mu$ m x 195 $\mu$ m with a pitch of 457 $\mu$ m and alternate pairs connected by a track. An  
21 inverse of this pattern is required on the substrate to create a complete electrical daisy chain  
22 connection. This inverse pattern was produced by printing a pattern of 600 $\mu$ m x 200 $\mu$ m x 200 $\mu$ m  
23 trenches in the substrate surface, filling the trenches with ICA, thermally curing the conductive  
24 material and finally, surface planarization. Interconnect features are then deposited at each end of  
25 the filled trenches with a pitch of 457 $\mu$ m, the result of which is shown in Figure 12(a). A bonding  
26 pressure of 8g was used before an additional thermal curing stage is conducted to cure the chip in  
27 place Figure 12(b) and (c). The chip can then be packaged using an identical embedding method to  
28 that presented in Figure 1, creating a fully encapsulated chip an example of which is shown in Figure  
29 12(d).  
30  
31  
32  
33  
34  
35  
36  
37  
38  
39  
40  
41  
42

43 Figure 12. Stages of flip chip packaging by multifunctional additive manufacturing  
44  
45

46 A four point probe was used to measure the contact resistance of interconnects via redistribution  
47 channels fabricated in the photopolymer substrate. An average resistance of 2.3 $\Omega$  was obtained  
48 between measurement pads with no change measured after the embedding and under filling  
49 process.  
50  
51

52 This flip chip packaging capability could be applied to the bottom layer of circuitry printed in  
53 complex substrates and embedded using the same method, allowing the photopolymer to act as an  
54 insulating underfill material protecting the chip itself and corresponding interconnects from external  
55  
56  
57  
58  
59  
60

1  
2  
3 mechanical stresses acting on the substrate itself. This demonstrates the high resolution capability of  
4 this hybrid process in its application to the packaging of electronic circuitry on a chip scale.  
5  
6

### 7 **Conclusion**

8  
9 A novel method for the production of multilayer embedded electronics by integrating additive  
10 manufacturing processes has been presented. DLP projection based stereolithography is used to  
11 manufacture an electronic substrate onto which conductors can be printed in an isotropic  
12 conductive adhesive. Surface mount electronic devices can subsequently be mounted on the ICA  
13 interconnects before they are thermally cured and packaged through an additional  
14 photopolymerisation stage.  
15  
16  
17

18  
19 A unique approach to the fabrication of z-axis through layer connections has been introduced,  
20 characterised and proven through the production of multiple demonstrators over two and three  
21 layers. Experimentation has shown that these freestanding pillars can be printed over a maximum of  
22 16 layers with an aspect ratio of 3.81. A combination of increasing print density of conductors and an  
23 increasing number of circuit layers alongside detailed print parameter investigation has facilitated  
24 the reduction in circuit footprint from 12mm x 12mm to 8mm x 8mm. The size of surface mount  
25 electronics and therefore, embedding layer thickness have also been halved.  
26  
27  
28  
29

30  
31 Demonstrators have been produced proving the use of integrated additive manufacturing  
32 technologies to create complex polymer structures with fully functioning internal multilayer  
33 electronics in the form of a flashing 555 timer circuit. The same encapsulation process has been  
34 applied to flip chip packaging, with dispensing of fine interconnect feature diameters as small as  
35 259 $\mu$ m at a pitch of 457 $\mu$ m.  
36  
37  
38  
39

40  
41 This technology has proven its potential to produce intricate electronic systems embedded within  
42 complex packages using a unique combination of additive manufacturing processes. Its digitally  
43 driven nature makes it ideal for iterative development of both its shape and function exhibiting its  
44 suitability for a variety of application areas including electronics packaging, lab on chip and condition  
45 monitoring.  
46  
47  
48

### 49 **Future Recommendations**

50  
51 The resolution of this process is limited by the particle size of commercially available low  
52 temperature isotropic conductive adhesive materials. The formulation of an ICA with smaller  
53 particles would allow the use of smaller nozzle IDs for dispensing and therefore a further reduction  
54 in size of conductors. This improvement in combination with the current DLP SLA process would  
55 result in a significant reduction in electronic footprint of embedded multilayer systems.  
56  
57  
58  
59  
60

## Acknowledgements

This work is funded by the UK Engineering and Physical Sciences Research Council under grants EP/L017431/1, EP/L017350/1, EP/L016907/1 and EP/L017415/1.

## References

- Andrzejewska, E., 2001. Photopolymerization kinetics of multifunctional monomers. *Progress in Polymer Science (Oxford)*, 26, pp.605–665.
- Anon, 2012. Obama Administration Announces New Public Private Partners. *www.whitehouse.gov*. Available at: <http://www.whitehouse.gov/the-press-office/2012/08/16/we-can-t-wait-obama-administration-announces-new-public-private-partners>.
- Borghino, D., 2015. Voxel8 Paves the Way for 3D-Printed Electronics. *Gizmag*.
- Gruber, H.F., 1992. Photoinitiators for free radical polymerization. *Progress in Polymer Science*, 17, pp.953–1044.
- Hull, C.W., 1986. Apparatus for Production of Three-Dimensional Objects by Stereolithography.
- Lipson, H. & Kurman, M., 2013. *Fabricated: The New World of 3D Printing*,
- Lopes, A. et al., 2006. Expanding Rapid Prototyping for Electronic Systems Integration of Arbitrary Form. In *Proceedings of the 17th Annual Solid Freeform Fabrication Symposium, University of Texas at Austin*. pp. 644–655.
- Lopes, A.J. et al., 2006. Integration of Direct-Write (DW) and Ultrasonic Consolidation (UC) Technologies to Create Advanced Structures with Embedded Electrical Circuitry. In *Proceedings of the 17th Annual Solid Freeform Fabrication Symposium, University of Texas at Austin, Austin, TX*. pp. 60–69.
- Lopes, A.J., MacDonald, E. & Wicker, R.B., 2012. Integrating stereolithography and direct print technologies for 3D structural electronics fabrication. *Rapid Prototyping Journal*, 18(2), pp.129–143. Available at: <http://www.emeraldinsight.com/10.1108/13552541211212113> [Accessed October 31, 2013].
- Niese, B. et al., 2014. Manufacturing of Conductive Circuits for Embedding Stereolithography by Means of Conductive Adhesive and Laser Sintering. *Physics Procedia*, 56, pp.336–344. Available at: <http://linkinghub.elsevier.com/retrieve/pii/S1875389214003241>.
- Palmer, J.A. et al., 2004. Rapid Prototyping of High Density Circuitry. In *Rapid Prototyping & Manufacturing 2004 Conference Proceedings*.
- Paulsen, J.A. et al., 2012. Printing conformal electronics on 3D structures with Aerosol Jet technology. *2012 Future of Instrumentation International Workshop (FIIW) Proceedings*, pp.1–4. Available at: <http://ieeexplore.ieee.org/lpdocs/epic03/wrapper.htm?arnumber=6378343>.
- Sharma, R., 2014. The Future of 3D Printing and Manufacturing. *Forbes*. Available at: <http://www.forbes.com/sites/rakeshsharma/2014/01/15/1255/>.

1  
2  
3  
4  
5  
6  
7  
8  
9  
10  
11  
12  
13  
14  
15  
16  
17  
18  
19  
20  
21  
22  
23  
24  
25  
26  
27  
28  
29  
30  
31  
32  
33  
34  
35  
36  
37  
38  
39  
40  
41  
42  
43  
44  
45  
46  
47  
48  
49  
50  
51  
52  
53  
54  
55  
56  
57  
58  
59  
60

Zhou, C. et al., 2013. Digital material fabrication using mask-image-projection-based stereolithography. *Rapid Prototyping Journal*, 19(3), pp.153–165. Available at: <http://www.emeraldinsight.com/10.1108/13552541311312148>.

Rapid Prototyping Journal

Table 1. Important properties of chosen conductive materials according to Epotek specifications

	<b>Epotek E4110-PFC (Material A)</b>	<b>Epotek EJ2189 (Material B)</b>
<b>Max. Particle Size (<math>\mu\text{m}</math>)</b>	$\leq 20$	$\leq 45$
<b>Viscosity (cPs)</b>	50000-60000	55000-90000
<b>Thixotropic Index</b>	3.3	5.2
<b>Curing Regimes</b>	1hr @ 120°C 3hr @ 80°C 6hr @ 45°C	15min @ 150°C 1hr @ 100°C 3hr @ 80°C 72hr @ 23°C
<b>Volume Resistivity (<math>\Omega\text{cm}</math>)</b>	$\leq 5 \times 10^{-3}$	$\leq 5 \times 10^{-3}$

Rapid Prototyping Journal

1  
2  
3  
4  
5  
6  
7  
8  
9  
10  
11  
12  
13  
14  
15  
16  
17  
18  
19  
20  
21  
22  
23  
24  
25  
26  
27  
28  
29  
30  
31  
32  
33  
34  
35  
36  
37  
38  
39  
40  
41  
42  
43  
44  
45  
46  
47  
48  
49  
50  
51  
52  
53  
54  
55  
56  
57  
58  
59  
60

1  
2  
3  
4  
5  
6  
7  
8  
9  
10  
11  
12  
13  
14  
15  
16  
17  
18  
19  
20  
21  
22  
23  
24  
25  
26  
27  
28  
29  
30  
31  
32  
33  
34  
35  
36  
37  
38  
39  
40  
41  
42  
43  
44  
45  
46  
47  
48  
49  
50  
51  
52  
53  
54  
55  
56  
57  
58  
59  
60

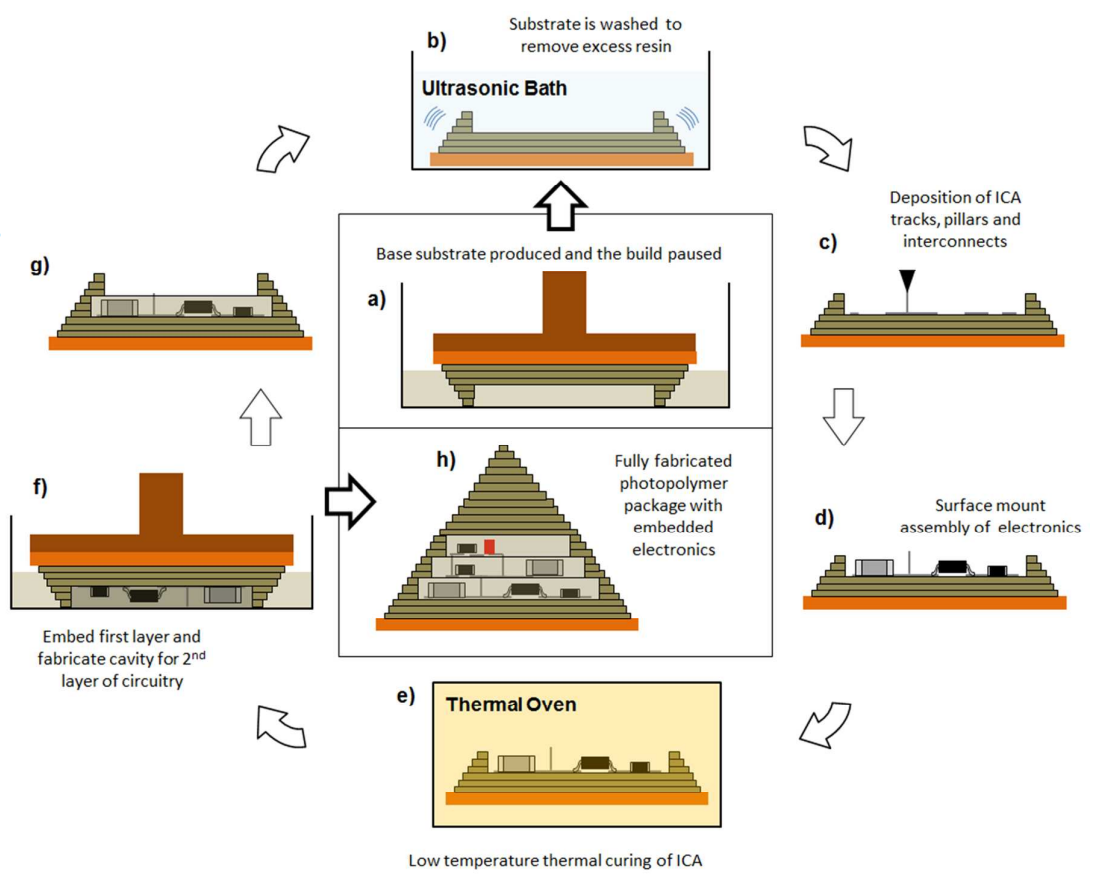


Figure 1. Overview of the hybrid additive manufacturing process

Rapid Prototyping Journal

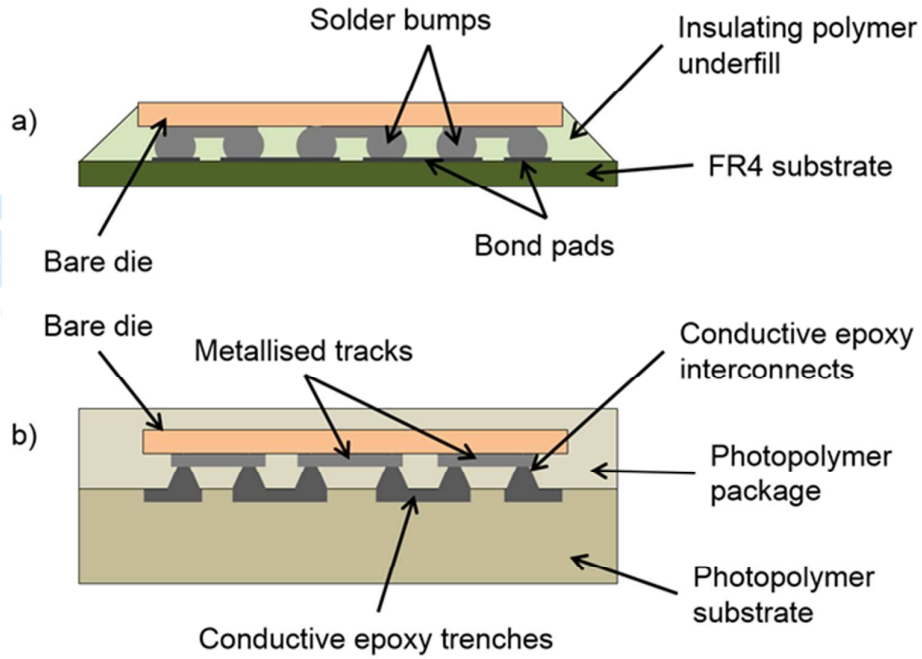


Figure 1. Comparison of flip chip packaging via a) conventional methods and b) hybrid additive manufacturing

1  
2  
3  
4  
5  
6  
7  
8  
9  
10  
11  
12  
13  
14  
15  
16  
17  
18  
19  
20  
21  
22  
23  
24  
25  
26  
27  
28  
29  
30  
31  
32  
33  
34  
35  
36  
37  
38  
39  
40  
41  
42  
43  
44  
45  
46  
47  
48  
49  
50  
51  
52  
53  
54  
55  
56  
57  
58  
59  
60

1  
2  
3  
4  
5  
6  
7  
8  
9  
10  
11  
12  
13  
14  
15  
16  
17  
18  
19  
20  
21  
22  
23  
24  
25  
26  
27  
28  
29  
30  
31  
32  
33  
34  
35  
36  
37  
38  
39  
40  
41  
42  
43  
44  
45  
46  
47  
48  
49  
50  
51  
52  
53  
54  
55  
56  
57  
58  
59  
60

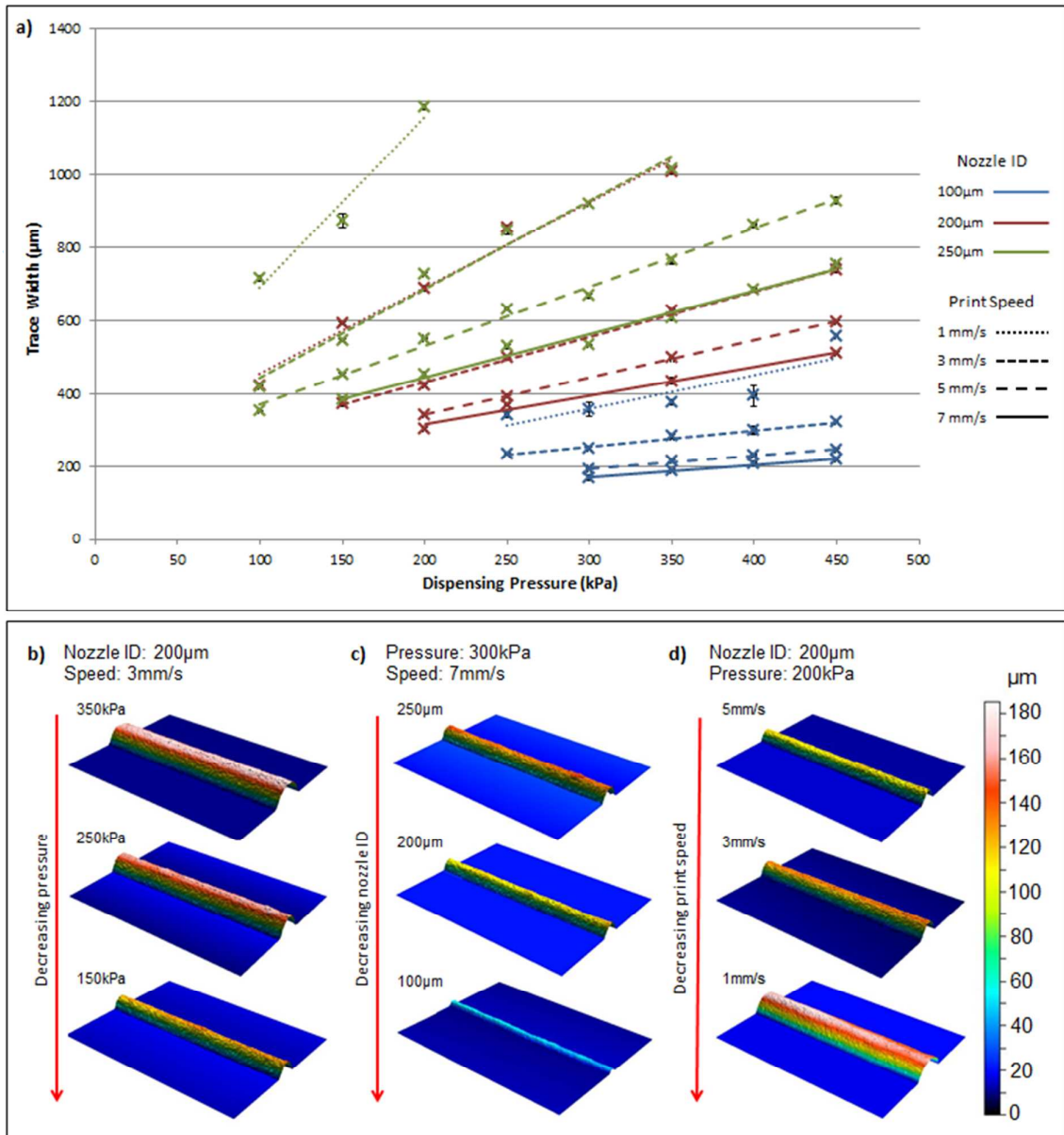


Figure 1. Effect of printing parameters on track width and appearance of material A

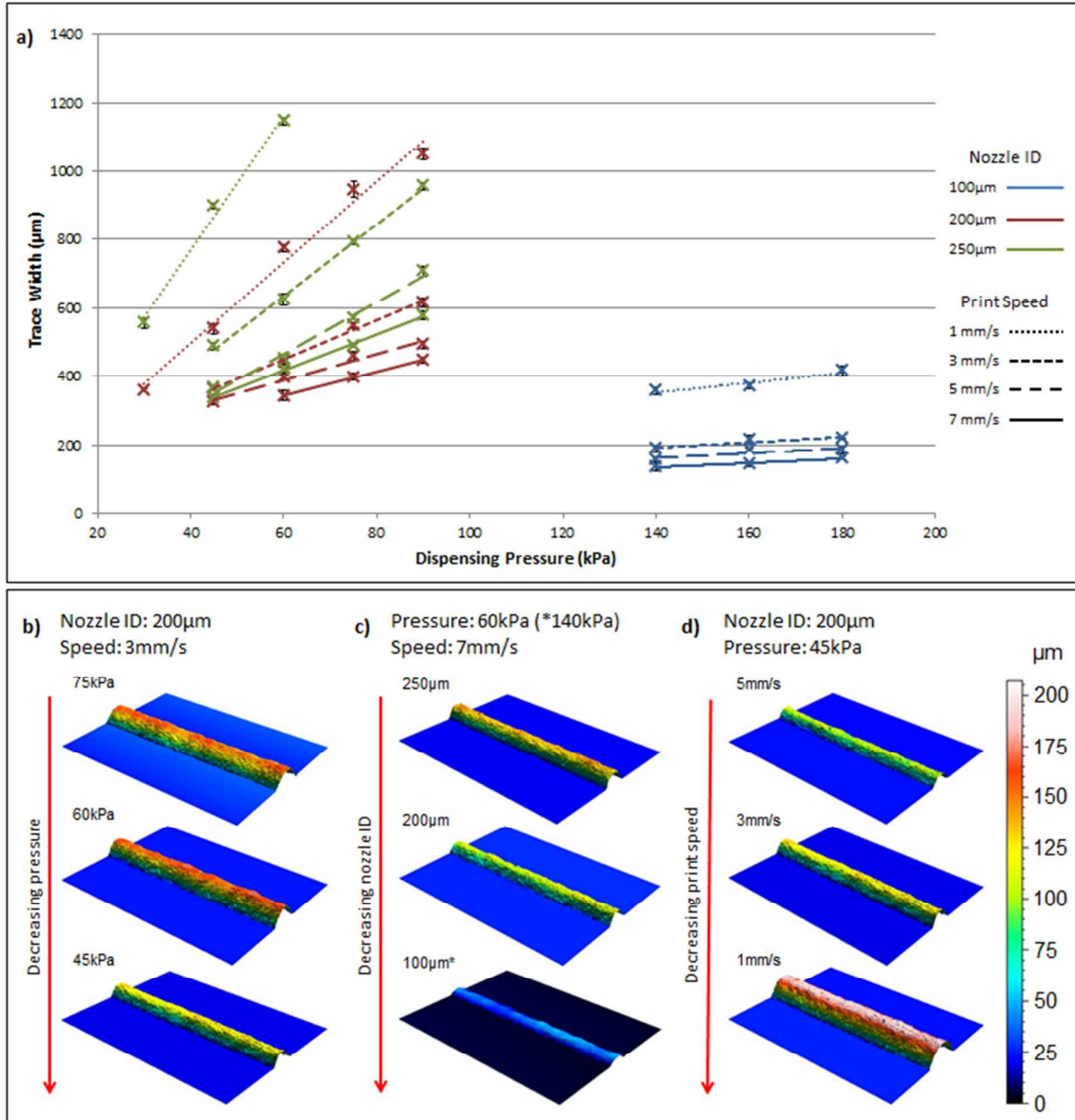


Figure 1. Effect of printing parameters on track width and appearance of material B

Journal

1  
2  
3  
4  
5  
6  
7  
8  
9  
10  
11  
12  
13  
14  
15  
16  
17  
18  
19  
20  
21  
22  
23  
24  
25  
26  
27  
28  
29  
30  
31  
32  
33  
34  
35  
36  
37  
38  
39  
40  
41  
42  
43  
44  
45  
46  
47  
48  
49  
50  
51  
52  
53  
54  
55  
56  
57  
58  
59  
60

1  
2  
3  
4  
5  
6  
7  
8  
9  
10  
11  
12  
13  
14  
15  
16  
17  
18  
19  
20  
21  
22  
23  
24  
25  
26  
27  
28  
29  
30  
31  
32  
33  
34  
35  
36  
37  
38  
39  
40  
41  
42  
43  
44  
45  
46  
47  
48  
49  
50  
51  
52  
53  
54  
55  
56  
57  
58  
59  
60

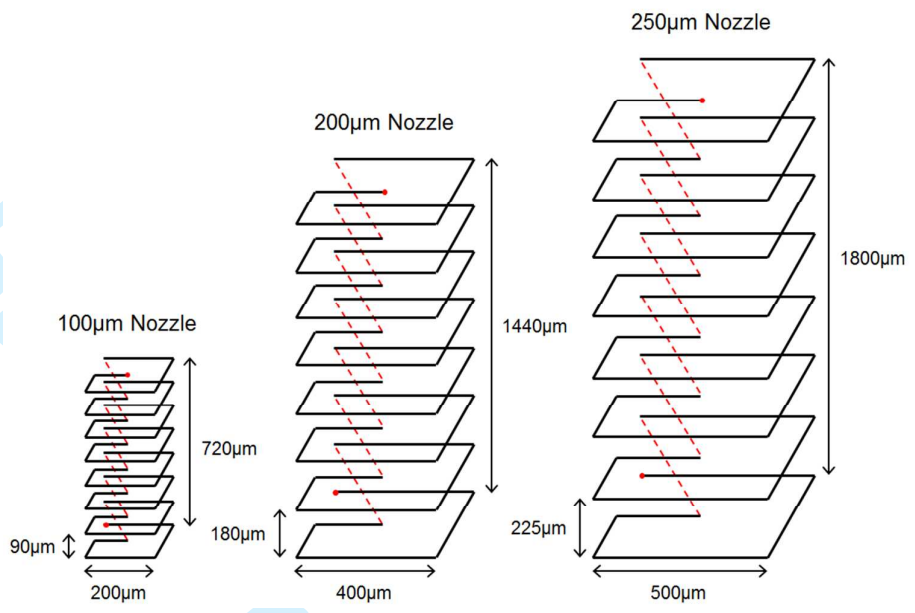


Figure 1. Freestanding pillar designs for each nozzle ID

Rototyping Journal

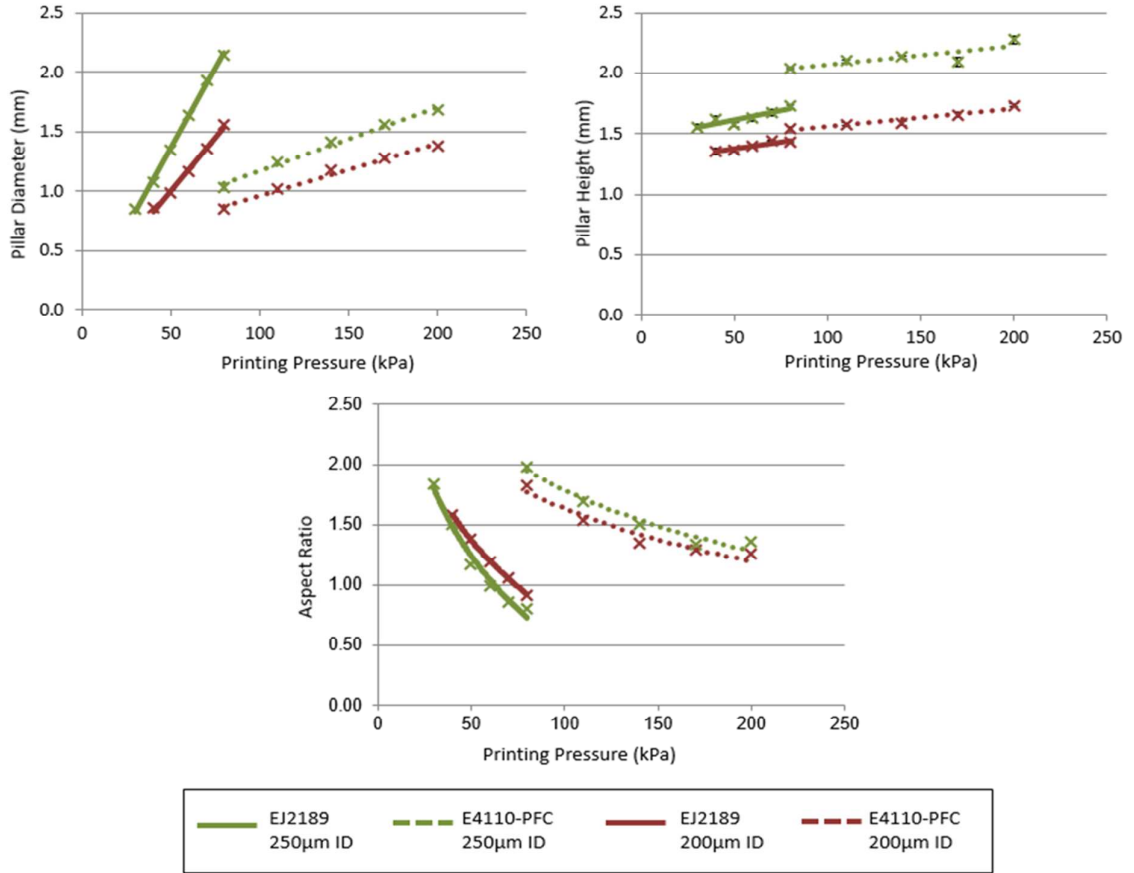


Figure 1. Diameters, height and aspect ratios of pillars produced in materials A and B using 250µm and 200µm nozzle IDs

1  
2  
3  
4  
5  
6  
7  
8  
9  
10  
11  
12  
13  
14  
15  
16  
17  
18  
19  
20  
21  
22  
23  
24  
25  
26  
27  
28  
29  
30  
31  
32  
33  
34  
35  
36  
37  
38  
39  
40  
41  
42  
43  
44  
45  
46  
47  
48  
49  
50  
51  
52  
53  
54  
55  
56  
57  
58  
59  
60

1  
2  
3  
4  
5  
6  
7  
8  
9  
10  
11  
12  
13  
14  
15  
16  
17  
18  
19  
20  
21  
22  
23  
24  
25  
26  
27  
28  
29  
30  
31  
32  
33  
34  
35  
36  
37  
38  
39  
40  
41  
42  
43  
44  
45  
46  
47  
48  
49  
50  
51  
52  
53  
54  
55  
56  
57  
58  
59  
60

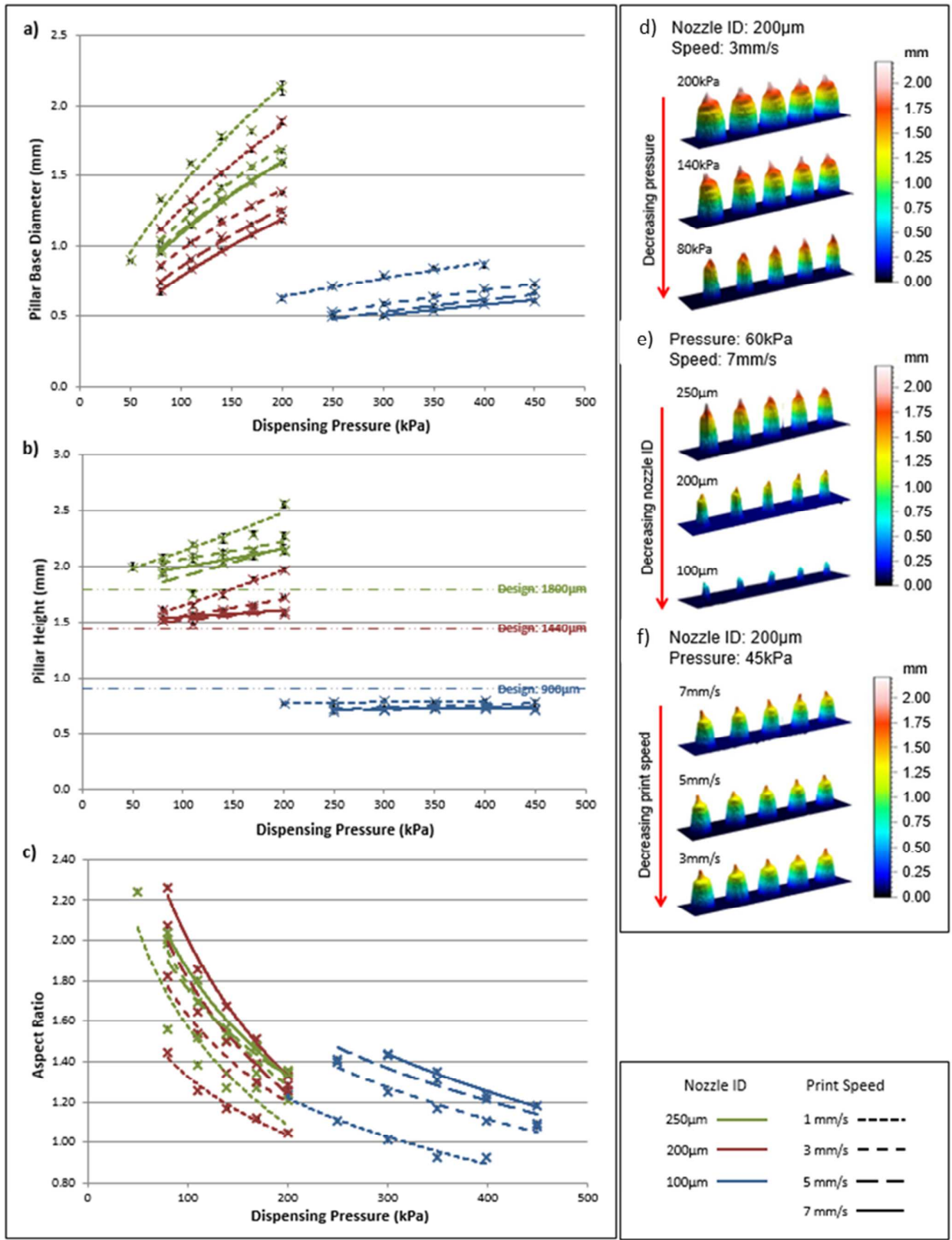


Figure 1. Graphic representation of effect of changing printing parameters on a) diameter, b) height and c) aspect ratio of profiles produced with decreasing d) pressures, e) nozzle sizes and f) print speeds

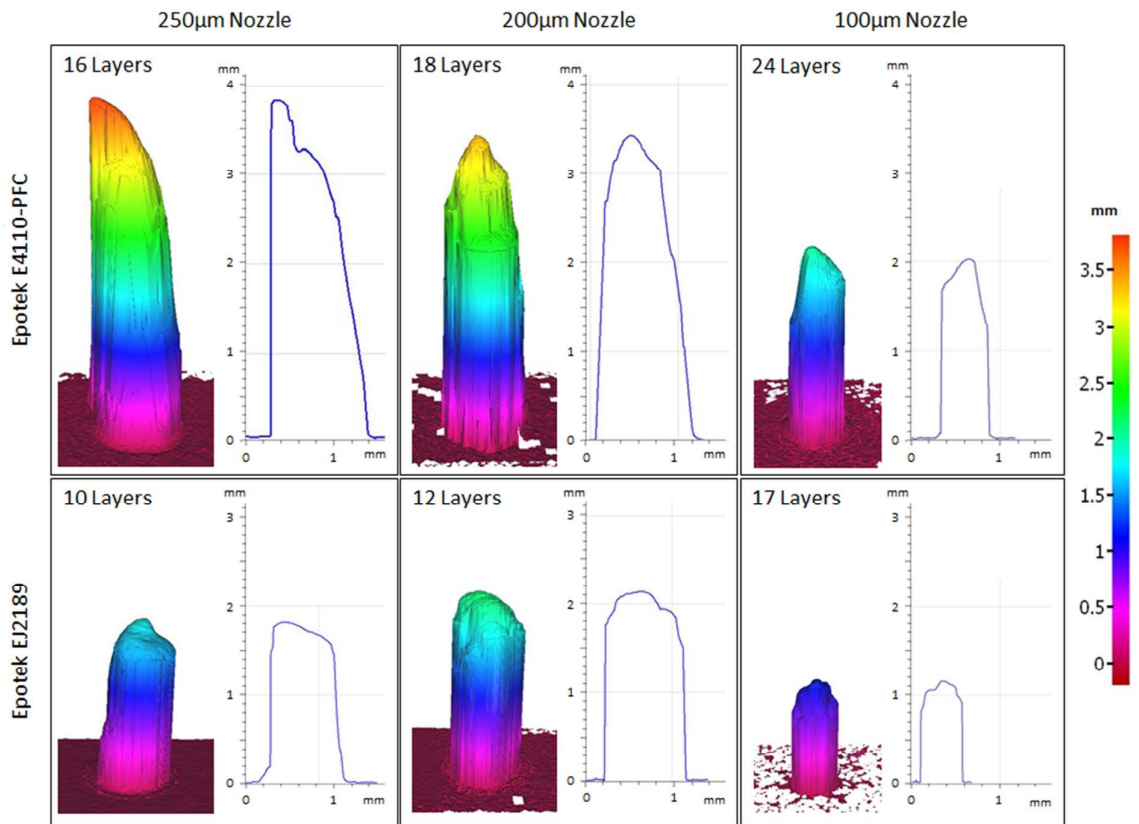


Figure 1. Comparison of largest achievable pillar structures using a combination of two materials and three nozzle sizes

1  
2  
3  
4  
5  
6  
7  
8  
9  
10  
11  
12  
13  
14  
15  
16  
17  
18  
19  
20  
21  
22  
23  
24  
25  
26  
27  
28  
29  
30  
31  
32  
33  
34  
35  
36  
37  
38  
39  
40  
41  
42  
43  
44  
45  
46  
47  
48  
49  
50  
51  
52  
53  
54  
55  
56  
57  
58  
59  
60

1  
2  
3  
4  
5  
6  
7  
8  
9  
10  
11  
12  
13  
14  
15  
16  
17  
18  
19  
20  
21  
22  
23  
24  
25  
26  
27  
28  
29  
30  
31  
32  
33  
34  
35  
36  
37  
38  
39  
40  
41  
42  
43  
44  
45  
46  
47  
48  
49  
50  
51  
52  
53  
54  
55  
56  
57  
58  
59  
60

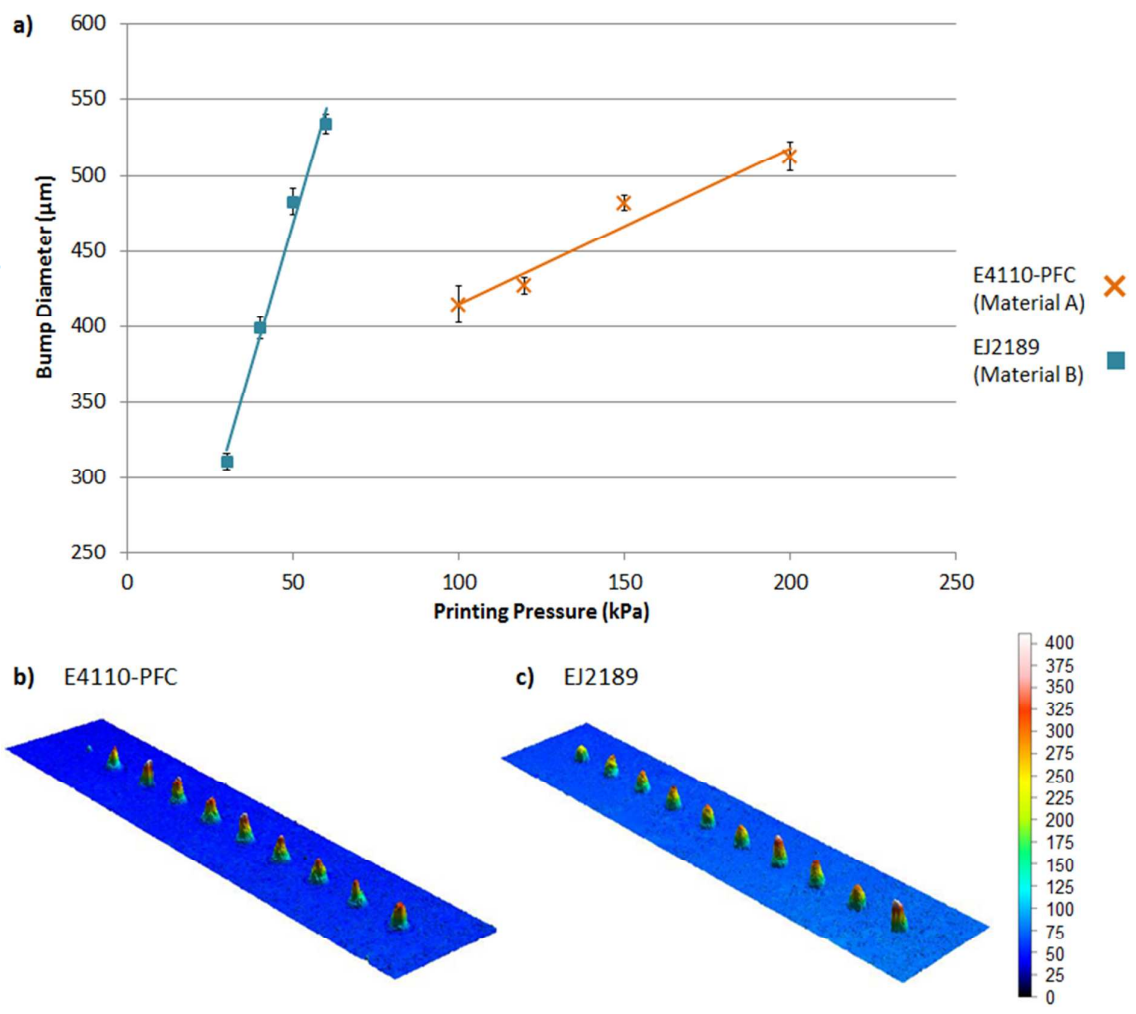


Figure 1. Comparison of interconnects printed in materials A and B

Rapid Prototyping Journal

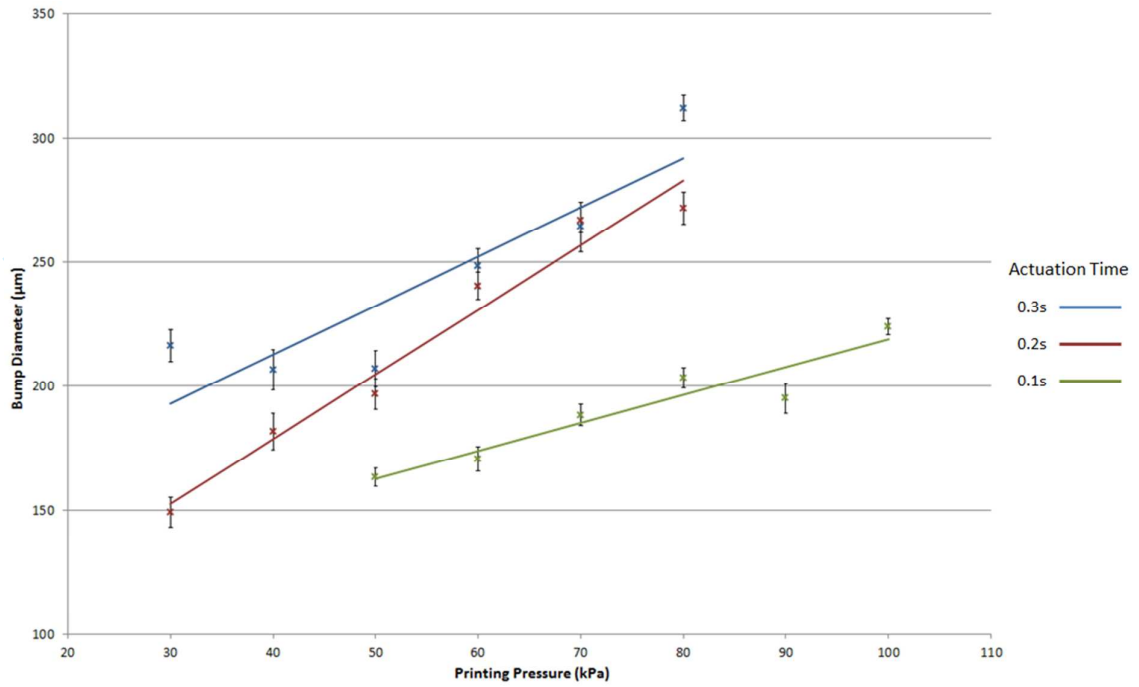


Figure 1. Relationship between printing pressure, actuation time and bump diameter at a 60µm print gap with a 100µm nozzle in material B

Rapid Prototyping Journal

1  
2  
3  
4  
5  
6  
7  
8  
9  
10  
11  
12  
13  
14  
15  
16  
17  
18  
19  
20  
21  
22  
23  
24  
25  
26  
27  
28  
29  
30  
31  
32  
33  
34  
35  
36  
37  
38  
39  
40  
41  
42  
43  
44  
45  
46  
47  
48  
49  
50  
51  
52  
53  
54  
55  
56  
57  
58  
59  
60

1  
2  
3  
4  
5  
6  
7  
8  
9  
10  
11  
12  
13  
14  
15  
16  
17  
18  
19  
20  
21  
22  
23  
24  
25  
26  
27  
28  
29  
30  
31  
32  
33  
34  
35  
36  
37  
38  
39  
40  
41  
42  
43  
44  
45  
46  
47  
48  
49  
50  
51  
52  
53  
54  
55  
56  
57  
58  
59  
60

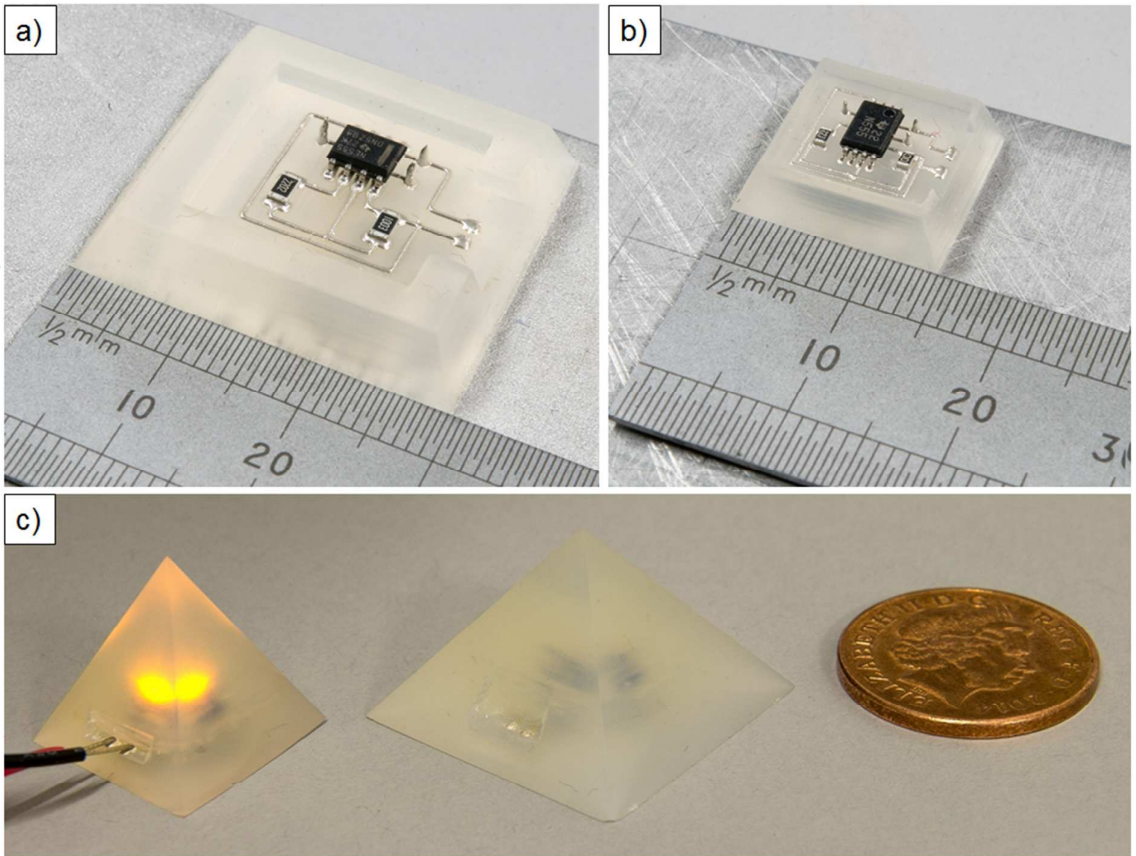


Figure 1. Comparison of demonstrator size reduction across three iterations

yping Journal

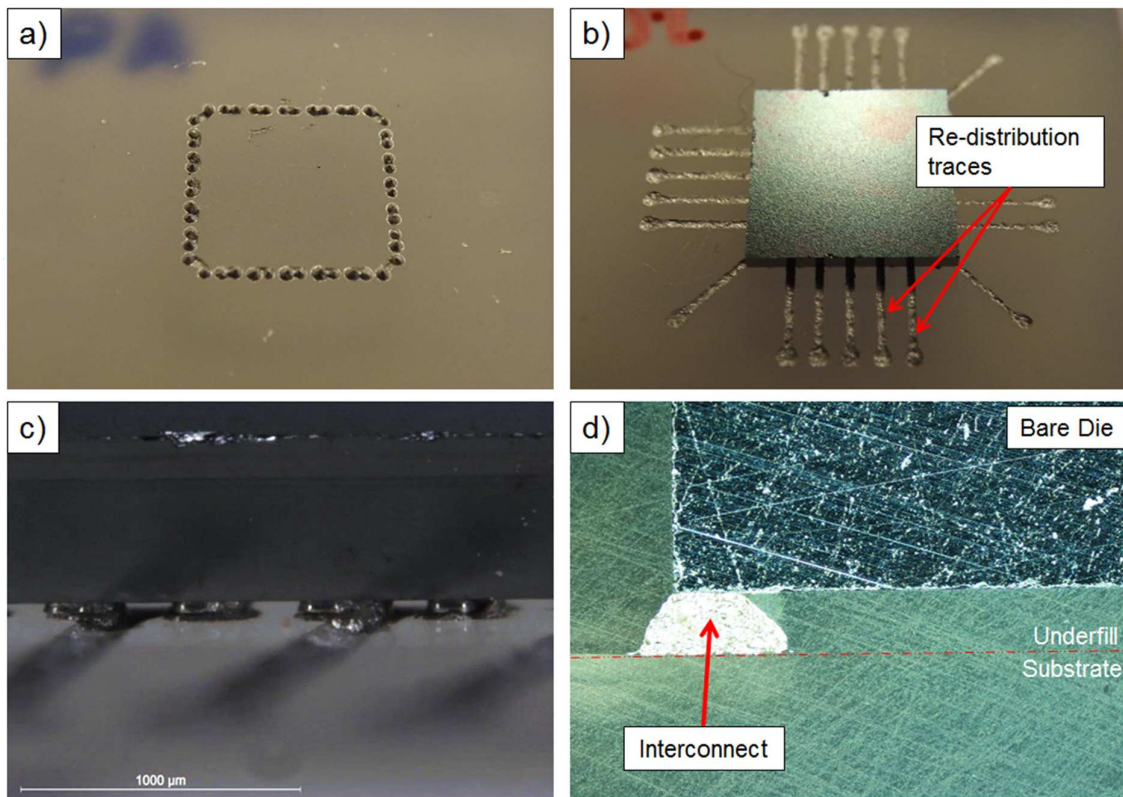


Figure 1. Stages of flip chip packaging by hybrid additive manufacturing

3D Printing Journal

1  
2  
3  
4  
5  
6  
7  
8  
9  
10  
11  
12  
13  
14  
15  
16  
17  
18  
19  
20  
21  
22  
23  
24  
25  
26  
27  
28  
29  
30  
31  
32  
33  
34  
35  
36  
37  
38  
39  
40  
41  
42  
43  
44  
45  
46  
47  
48  
49  
50  
51  
52  
53  
54  
55  
56  
57  
58  
59  
60